RSC Applied Polymers

ROYAL SOCIETY OF CHEMISTRY

PAPER

View Article Online
View Journal | View Issue

Cite this: *RSC Appl. Polym.*, 2025, **3**, 97

Investigation of the influence of substituents on the dielectric properties of polyethylene derivatives†

Bing Zhong,[a,b] Yin Zhang,[a,b] Wei You *[a,b] and Yu Wang *[a]

To systematically explore the influence of microscopic substituent structures on the macroscopic dielectric properties of polyethylene (PE), ten PE derivatives, incorporating 18 mol% of diverse functional groups such as halogens, azides, norbornene-based groups, and macrocyclic structures, were synthesized using post-functionalization reactions from the same poly(ethylene-*co*-vinyl acetate) precursors. Using linear low-density PE (LLDPE) as a reference, the experimental results reveal the effective modulation of the dielectric constants of PE derivatives by introducing various functional groups. The PE units in the molecular chain ensure excellent compatibility of PE derivatives with LLDPE to form homogeneous polymer blends in molten states. Blending with LLDPE effectively reduces the dielectric loss of PE derivatives and exhibits a higher dielectric constant than LLDPE at the frequencies below 10 Hz. Notably, these blends exhibited a more pronounced temperature dependence of the dielectric constants, indicating higher values at elevated temperatures. More importantly, the dielectric breakdown strength of the blends was effectively enhanced, reaching up to 1.4 times that of LLDPE. In addition, improvements in the mechanical properties of the blends were also observed with the strain-at-break exceeding 1000%. This research confirms that post-polymerization functionalization provides an excellent platform to systematically evaluate the influence of substituents on synthetic polymers, and it is expected to generate new insights into the mechanisms of enhancing polymer dielectric properties.

Received 31st March 2024,
Accepted 18th June 2024

DOI: 10.1039/d4lp00117f

rsc.li/rscapplpolym

Introduction

Dielectric polymers manifest electrical properties through the polarization within their molecular chains,[1] which is the finite displacement of the electron cloud density of the dipoles, resulting in the formation of a net dipole moment when subjected to an electric field. These polymers have garnered significant attention and found applications in diverse fields, including film capacitors, electronic communications, and energy storage materials,[2–5] owing to their characteristics of high flexibility, low density, and repeated processability.[6,7] The polarizability of macromolecules is commonly assessed using the dielectric constant (ε'), wherein a higher ε' represents a larger net dipole moment of the macromolecule. For instance, poly(vinylidene fluoride) (PVDF), containing high dipole moment C–F bonds, can exhibit a ε' of $\geq$10,[8–10] making it and its copolymers suitable for use in capacitors and piezoelectric and ferroelectric materials.[11–15] On the other hand, biaxially oriented polypropylene (BOPP) films, demonstrating both a low ε' and a low dielectric loss (ε''),[4,10,12] have been employed as electronic circuit components to meet the requirements of high electric field strengths and high frequencies.

The polarization behavior of dielectric polymers is characterized by a multiscale nature, responding to a multilevel motion/relaxation process. This process encompasses electronic polarization (the relative displacement of the electron cloud), atomic polarization (the induced dipole moment between the centers of positive and negative charges), ionic polarization, dipolar (or orientational) polarization, and inter-

[a]*Beijing National Laboratory for Molecular Sciences (BNLMS), CAS Key Laboratory of Engineering Plastics, Institute of Chemistry, Chinese Academy of Sciences, Beijing, 100190, China. E-mail: ywang507@iccas.ac.cn, weiyou@iccas.ac.cn*
[b]*University of Chinese Academy of Sciences, Beijing 100049, China*

†Electronic supplementary information (ESI) available: Additional data of TGA, dielectric measurement, mechanical experiments for the PE derivatives and their blends. The determined elemental composition in the PE-Br/LLDPE, PE-I/LLDPE, and PE-OPh/LLDPE blends. The comparison of 1-D WAXD curves of the obtained PE derivatives and the blends from PE-Br/LLDPE to PE-OPh/LLDPE. The 1-D SAXS plots of the PE derivatives PE-Br, PE-I, and PE-OPh at room temperature. The engineering stress–strain plots of the obtained PE-Br, PE-I, PE-OPh and their blends from PE-Br/LLDPE to PE-OPh/LLDPE. Temperature dependence of the dielectric properties of PE-Br, PE-I, LLDPE, PE-I/LLDPE, and PE-OPh/LLDPE. The cooling and second heating DSC traces of LLDPE, PE-Br, PE-I, PE-OPh and their blends (PE-Br/LLDPE, PE-I/LLDPE, and PE-OPh/LLDPE) after quenching from 200 °C at a rapid rate of 50 °C min^{-1}. See DOI: **https://doi.org/10.1039/d4lp00117f**

facial polarization on the phase domain boundaries (or the matrix–filler boundaries).[3] In other words, the macroscopic dielectric properties of polymers and their composites result from the co-coupling microstructures at various scales, including the chemical structures of repeating units,[9,16,17] molecular chain conformation,[14,18] crystal forms,[13,19] microphase separation,[20,21] filler dispersion,[22] *etc.*

Over the past few decades, numerous studies have investigated methods to tune the dielectric properties of polymer-based materials. Generally, the ε' of polymeric materials can be enhanced through three main approaches: modifying the structure of polymer backbones and substituents,[13,23,24] modulating the microstructures with an external field,[19,25,26] and incorporating inorganic fillers.[27–29] Among these, structural design is fundamental and crucial, influencing both microstructures and the interaction between the polymer matrix and inorganic fillers. Zhu *et al.* successfully increased the ε' of poly (methyl methacrylate) from 3.3–4.0 to 11.4 by introducing a sulfone group (–SO_2–) with a high dipole moment while maintaining a low ε''.[23] Furthermore, the discharge energy density of this material tripled.[23] The introduction of a trifluoroethylene comonomer into the poly(vinylidenefluoride) (PVDF) molecular chain to prepare a random copolymer P(VDF-TrFE) has been shown to enhance its piezoelectric coefficient and electromechanical coupling coefficient.[13,24,30] Additionally, a further enhancement in the piezoelectric coefficient was reported, reaching 1000 pm V^{-1} for the prepared P(VDF-TrFE-CEF-FA) containing ≤2 mol% fluorinated alkyne (FA) comonomer, comparable to that of the representative ceramic oxidized material ZNT.[31]

The dielectric properties of the polymer undergo changes corresponding to alterations in the microstructures. For instance, among all the crystal phases of PVDF,[32–35] the β crystal phase, with the largest net dipole moment, demonstrates the highest ε' and the most pronounced dielectric properties.[11] The induction of microstructures with high dipole moments through an externally applied field to enhance polarization is a topic that has garnered significant attention. Ma and his co-workers investigated the mechanisms of shear-induced β-crystal formation in PVDF,[25,26] revealing that ionic interactions contribute to the formation of shear-induced β and γ crystals.[36] It was also reported that β phases can be induced by uniaxial elongation, resulting in higher dielectric properties.[37] Drawing from the study of various polyamides (PAs) with different chemical structures (such as PA610, PA612, PA1010, and PA1212), it was observed that higher crystallinity promotes the ferroelectric properties.[19] Liang, Liu, and their colleagues demonstrated that thermoplastic polyurethane elastomers, featuring evident microphase separation, exhibited a high ε' through changes in the species of the hard segments.[21] However, the chemical structure of polymers significantly influences their microstructures. Considering the random copolymer poly(ethylene-*co*-vinyl acetate) (EVA), which consists of ethylene and vinyl acetate monomers, variations in the content of vinyl acetate led to changes in the crystal phase, chain dynamics, ε', and ε''.[38,39]

Incorporating inorganic nanofillers with high energy density and ε' into flexible polymer materials is a crucial approach for enhancing the dielectric properties of polymer-based devices, such as film capacitors.[27,28] This approach involves an increase of ε' through accumulated dipoles at the boundaries of phase domains, known as interfacial polarization, observed in both polymer blends and nanofiller-reinforced systems.[29,40] Interfacial compatibility between the polymer matrix and the filler plays a pivotal role in determining filler dispersion and, consequently, the device's performance.[29,41] However, incorporating inorganic nanofillers into non-polar polymers such as polyethylene (PE) to increase ε' poses significant challenges due to compatibility issues, leading to non-uniform filler distribution.

PE, as one of the most extensively manufactured polymers, exhibits one of the lowest dielectric constants among bulk materials, making it an ideal substrate for investigating the influence of substituents on polymer dielectric properties. Despite recent advancements in methods for preparing polar-group-functionalized PE derivatives, a comprehensive exploration of their dielectric properties is yet to be undertaken. This shortfall can be attributed to the inherent challenges associated with directly copolymerizing ethylene and polar vinyl monomers, wherein simultaneous control over functional group incorporation, distribution, and molecular weight proves elusive.[42] Recently, our group reported a post-functionalization approach based on Mitsunobu reactions to efficiently synthesize a series of functional PE derivatives from commercial EVA precursors.[43–45] Notably, the functionalization conditions do not need transition metal catalysts. More importantly, the complete conversion of functional groups ensures that the functional group contents, distribution, and molecular weight of the resulting PE derivatives are dictated by the EVA starting materials, thus providing a good platform to systematically study the influence of substituents on polymer properties. In this work, ten PE derivatives were synthesized (as shown in Scheme 1) to explore the structure–property relationship of dielectric polymers and provide guidance for enhancing the dielectric properties of polyolefins. The functional groups varied from halogens (–Br and –I) to phenyl ethers, azides, macrocyclic structures and norbornene-based groups, while the main chain structures and functional group contents among the ten samples remained the same. The substituents used in this study have two main advantages. Firstly, their intrinsic dipole moments and steric barriers vary depending on the chemical structure. Secondly, some substituents are expected to enhance the potential applications of the polymers. For example, the introduction of polar groups such as Br– and I– into the polymer backbones can effectively affect the energy density and efficiency of polymeric capacitors used for energy storage.[46] On the other hand, aromatic- and aliphatic-ring substituents are expected to affect the band gap and T_g of the materials, which are important factors in determining the dielectric breakdown strength.[47,48] Through a comparative analysis of these ten PE derivatives, we aim to unveil the influence of substituents on both the microstructure and

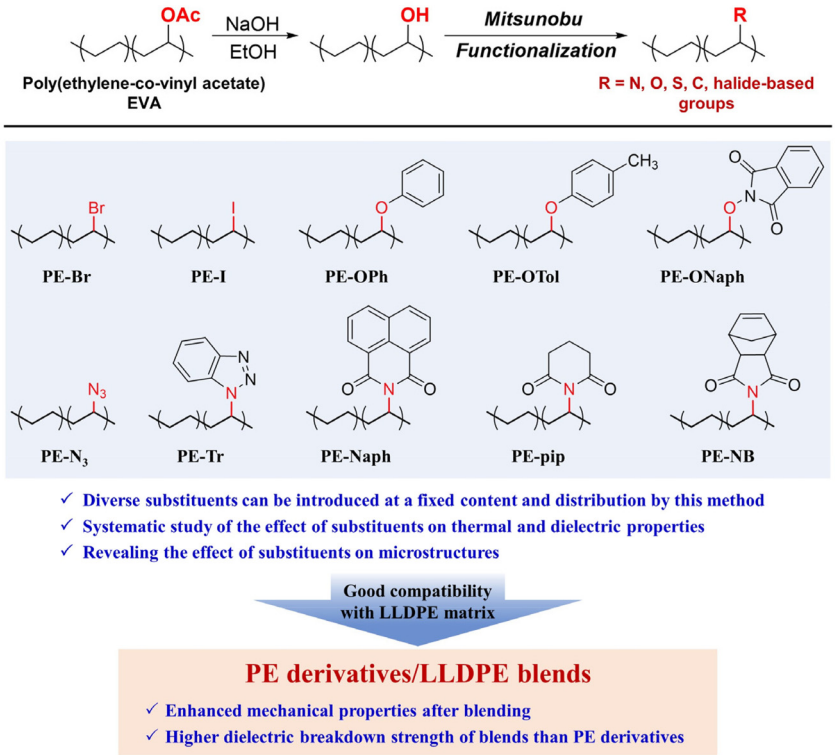

Scheme 1 General route for preparing PE derivatives from the Mitsunobu reaction (top), and the chemical structures of ten products used in this study. The PE backbone ensures good compatibility between the resulting PE derivatives and LLDPE, facilitating the preparation of their blends.

macroscopic dielectric properties. Additionally, the PE units in the molecular backbone ensure good compatibility between the synthesized PE derivatives and PE materials. By melt blending, a small amount of PE derivatives effectively enhanced the dielectric and mechanical properties of the linear low-density PE (LLDPE) matrix, particularly the dielectric breakdown strength and the strain-at-break.

Experimental section

Materials

EVA with a vinyl acetate content of 40 wt% (= 18 mol%) was purchased from Aladdin Co., Ltd Shanghai, China. Its melt flow index was determined to be 52 g per 10 min at 190 °C under a 2.16 kg load according to ASTM D1238. The polyethylene derivatives were prepared according to our previously reported Mitsunobu-functionalization method.[43] The functionalization achieved complete conversion as confirmed by FT-IR and NMR characterization.[43] The synthesis procedure, along with the obtained NMR and FT-IR spectra of the PE derivatives shown in Scheme 1 (except for PE-OTol, which is described in the ESI, and its NMR and FT-IR spectra are provided in Fig. S1–S3†), is referenced elsewhere.[43]

Preparation of PE derivatives/LLDPE blends

To investigate the compatibility of the obtained PE derivatives PE-Br, PE-I, and PE-OPh, as shown in Scheme 1, with the polymer matrix and the effect on their dielectric properties, commercial linear low-density poly(ethylene) (LLDPE, Macklin Inc. Shanghai, China) with a melt flow index of 2 g per 10 min at 190 °C under a 2.16 kg load was used as a matrix to prepare the blends. The PE-Br/LLDPE, PE-I/LLDPE, and PE-OPh/LLDPE blends (with a PE derivative content of 5.9 wt%) were prepared by a melt-mixing method using a co-rotating twin screw extruder-kneader (Haake MinLab II, Thermo Fisher Scientific) with a screw rotation speed of 30 rpm at 180 °C.

Characterization of thermal properties

The glass transition (T_g), crystallization (T_c), and melting (T_m) temperatures were determined from the cooling and second heating traces by using differential scanning calorimetry (DSC Q200, TA Instruments Inc.) over −130 to 200 °C under a nitrogen atmosphere. The heating and cooling rates are 10 °C min^{-1}. Thermal stability was evaluated by using thermogravimetric analysis (TGA 8000, PerkinElmer) from 50 to 600 °C at a heating rate of 20 °C min^{-1}. The degradation onset temperature and the temperature corresponding to the peak in the first-order derivative curve are represented by T_d and T_{peak}, respectively.

X-ray measurements

The wide-angle X-ray diffraction (WAXD) and small-angle X-ray scattering (SAXS) experiments were conducted on a Xeuss 2.0 WAXD/SAXS system (Xenocs SA). X-ray radiation was generated

using a Cu Kα X-ray source with a wavelength of 1.5418 Å (GeniX3D Cu ULD). The used sample-to-detector distances were 150 mm and 2500 mm for WAXD and SAXS measurements, respectively. All of the films of the synthesized PE derivatives and their blends (with a thickness of *ca.* 0.5 mm) were obtained by melting them at 180 °C and hot pressing at 5 MPa for 3 min, followed by quick cooling to room temperature under compression. A semiconductor detector (Pilatus 300k, DECTRIS) with a resolution of 487 × 619 pixels (pixel size of 172 × 172 μm^2) was used to collect 2-D WAXD/SAXS patterns, with selected acquisition times of 300 s and 900 s, respectively. The 1-D intensity profiles were integrated from the background-corrected WAXD/SAXS patterns, which are corrected for detector noise, air scattering, and sample absorption.

Characterization of dielectric properties

The dielectric constant (ε') and loss (ε'') of PE derivatives and their blends were measured in the temperature range of 0–120 °C at 20 °C intervals using broadband dielectric spectroscopy with the Quatro temperature control system and a cryostat under a nitrogen atmosphere, and the temperature accuracy was maintained within ±0.1 °C. The broadband dielectric spectroscopy system included a low-frequency module (Alpha-A High Performance Frequency Analyzer) and a high-frequency module (Agilent E4991A RF Impedance/Material Analyzer). Disk samples with a diameter and thickness of 20 mm and approximately 100 μm, respectively, were cut from the hot-pressed films (melted at 180 °C and then pressed at 5 MPa for 3 min) and secured between parallel plate electrodes. A frequency sweep ranging from 10^7 to 10^{-2} Hz was conducted at each temperature, with a ramp rate of 10 °C min^{-1} to transition to the next measurement temperature. The dielectric breakdown strength (ε_b) of the samples with a thickness of *ca.* 0.5 mm was determined by applying an increasing electrical field using a high voltage power supply at a boost rate of 20 V s^{-1} at 25 °C and RH 30% until breakdown. Measurements were repeated ten times for each sample.

Morphology observation

The morphology of the as-prepared blends PE-Br/LLDPE, PE-I/LLDPE, and PE-OPh/LLDPE with sputtering platinum (thickness of *ca.* 4 nm) was observed by scanning electron microscopy (SEM, Hitachi SU-8020) under an accelerated voltage of 10 kV. Elemental distribution was characterized using energy dispersive spectroscopy (EDX GENESIS).

Tensile testing

Thin tensile strips (10 mm width, 150 mm length, and *ca.* 0.1 mm thickness) were cut from the hot-pressed film (melted at 180 °C and then pressed at 5 MPa for 3 min). The plots of engineering stress *versus* engineering strain were obtained using Instron 3365 at a constant crosshead speed of 6 mm min^{-1}. All measurements were repeated five times for each sample.

Dynamic mechanical analysis (DMA)

A DMA (Q800, TA Instruments) was used to record the temperature dependence of dynamic storage (E') and loss (E'') moduli from −130 to 90 °C at a rate of 3 °C min^{-1} under 1 Hz, with a given strain of 0.1%. The strip sample dimensions were 25 mm/3 mm/0.5 mm (length/width/thickness). The $T_{g,DMA}$ was determined by the peak temperature of E''.

Results and discussion

Synthesis and characterization of PE derivatives *via* the Mitsunobu reaction

In this study, EVA with a vinyl acetate content of 18 mol% was selected to prepare the PE derivatives, conferring a high degree of functionalization while maintaining PE-like backbones. The sequential alcoholysis and Mitsunobu (or Appel) functionalization do not affect the functional group contents and polymer chain lengths. Consequently, ten products shown in Scheme 1 were successfully prepared, featuring 18 mol% functionalization with diverse groups, ranging from halogens (–Br and –I) to phenyl ether, azides, macrocyclic structures and norbornene-based groups. Most of the products are challenging to be prepared by traditional direct copolymerization approaches, and the ^{1}H, ^{13}C NMR, and FT-IR spectra were identical to our previous report.[43]

The influence of functional groups on the characteristic temperatures such as T_g, T_c, and T_m of the semi-crystalline PE derivatives (excluding the amorphous PE-ONaph, PE-pip, and PE-NB) was compared by the DSC cooling/heating traces (Fig. 1). Using LLDPE with saturated C–H bonds as a basis for comparison, it was found that the T_c, T_m, and their corresponding enthalpy changes (ΔH_c and ΔH_m) gradually decreased as the steric barrier of functional groups increased (see PE-Br, PE-I, PE-OPh, and PE-OTol in Table 1), indicating a deterioration in crystallization ability. Additionally, PE-ONaph, PE-pip, and PE-NB were amorphous polymers without crystallization and melting peaks in the DSC traces. Their glass transition steps are shown in Fig. S4.† TGA curves (shown in Fig. S5†) revealed a two-stage weight loss for certain PE derivatives, namely PE-OPh, PE-OTol, PE-ONaph, PE-Nr, and PE-pip, exhibiting corresponding two T_ds and T_{peak}s (listed in Table 1). In the case of PE-Naph and PE-NB, even three stages of weight loss were detected, suggesting a more complex thermal degradation behavior among the studied PE derivatives. Notably, the first T_d of the PE derivatives with multiple weight loss stages is lower than the single T_d of LLDPE, suggesting that the functional groups degrade more rapidly than the PE backbone.

Not only does the thermal stability vary with the functional groups, but the unit-cell structure of the synthesized PE derivatives also differs. In the 1-D WAXD curve of LLDPE, two diffraction peaks located at 2θ = 21.4° and 23.7° suggest a typical orthorhombic unit cell (Fig. S6†). However, the 1-D WAXD curves of PE-I and PE-Naph differ significantly from that of LLDPE. Both of them exhibit more than three diffraction peaks, as shown in Fig. S6.† It has been reported in the litera-

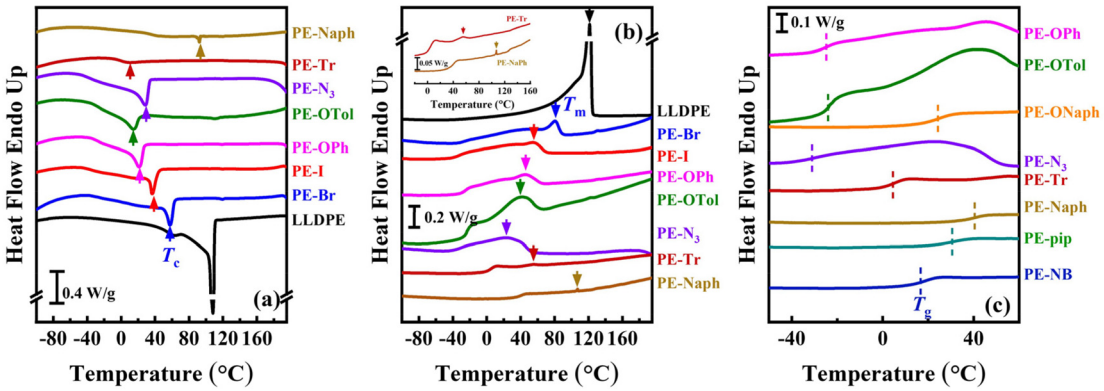

Fig. 1 DSC traces of selected PE derivatives during (a) cooling and (b) second heating. A reference for comparison is provided with LLDPE featuring saturated C–H bonds (black line). The determined crystallization and melting temperatures are indicated by the arrows. An enlargement of the second heating traces of PE-OPh and PE-Naph is shown in the inset to demonstrate their weak melting peaks. (c) The glass transition temperature was determined by the step in the second heating traces and is labelled by a dashed line.

Table 1 Determination of the thermal properties of the resulting PE derivatives

Sample	T_g (°C)	T_c (°C)	ΔH_c (J g^{-1})	T_m (°C)	ΔH_m (J g^{-1})	T_d [b] (°C)
LLDPE	N.D.[a]	107.4	89.3	120.6	90.8	440.6
PE-Br	N.D.	57.5	31.8	80.5	29.5	446.7
PE-I	N.D.	36.5	27.9	53.4	26.8	421.0
PE-OPh	−24.4	20.9	25.6	45.0	17.8	229.2, 448.7
PE-OTol	−22.7	14.3	18.3	42.5	17.4	221.6, 462.1
PE-ONaph	24.6	N.D.	N.D.	N.D.	N.D.	236.0, 451.2
PE-N_3	−30.3	25.7	27.1	26.0	28.7	221.0, 397.8
PE-Tr	4.7	9.9	5.2	54.4	4.7	391.6
PE-Naph	41.1	92.3	1.3	107.2	1.4	218.7, 272.4, 412.3
PE-pip	31.5	N.D.	N.D.	N.D.	N.D.	253.9, 476.9
PE-NB	19.0	N.D.	N.D.	N.D.	N.D.	227.7, 363.4, 467.2

[a] N.D. denotes not determined. [b] Multiple peaks were detected in some samples.

ture that the addition of halogen groups can alter the crystalline structure of the PE backbone.[49] On the other hand, for PE-N_3 with azide groups, only a single diffraction peak at 2θ = 20.9° was found, implying the induction of a hexagonal unit cell of LLDPE (Fig. S6†).[50] The hexagonal phase of PE is usually obtained under high temperature, high pressure, or physical treatments. In our work, the functional groups affect the unit cell structure and chain conformation, in agreement with the previous literature.[49–51] The differences in the unit cell are likely responsible for the high T_c and T_m of PE-Naph.

Effect of functional groups on the dielectric properties of PE derivatives

Restricted by the polymerization routes, current literature results make it difficult to comprehensively compare various types of functional groups, especially the complex macrocyclic groups. Our post-functionalization route, based on the Mitsunobu reaction, not only significantly shortens material preparation cycles but also avoids the drawback of altering the distribution of functional groups in the main chain during traditional direct addition copolymerization, providing a more solid foundation for this study.

In Fig. 2, double logarithmic plots of ε' ((a) and (b)) and ε'' ((c) and (d)) *versus* frequency measured at 23 °C for each PE derivative are illustrated. The results clearly demonstrate that the ε' of PE derivatives can be effectively modulated by introducing functional groups (see the dielectric properties in Table S1†). For instance, the plots of PE-OTol and PE-Naph closely resemble that of LLDPE, while the ε' of PE-N_3 remains above 5.0 over a wide frequency range. Remarkably, the ε' at low frequencies (10^{-2}–10^{-1} Hz) can be enhanced by more than one or two orders of magnitude by inserting the –Br and –I groups (PE-Br and PE-I). Although the ε' of the semi-crystalline product PE-I decreases rapidly with increasing frequency, it still surpasses 3 up to 10^5 Hz, which is higher than those of many reported systems.[9,10,52] Furthermore, these results confirmed the advantages of our post-functionalization route in investigating the effect of subtle chemical structure differences on the dielectric properties of polymeric materials. For example, the additional methyl group on the branched chain of PE-OTol, compared to PE-OPh, results in a decrease in its ε' from approximately 3 to *ca.* 2 (see Fig. 2(a)). Compared to PE-N_3, the introduction of benzene not only reduces the ε' of PE-Tr but also affects the dielectric relaxation behaviors as illustrated by the ε' and ε'' plots shown in Fig. 2(b) and (d). The ε'' peak shifting toward low frequency for PE-Tr compared to PE-N_3 in Fig. 2(d) implies that benzene delays the relaxation. To clarify whether the relaxation behavior observed in Fig. 2(c) and (d) is due to whole chain relaxation or segment relaxation, the semi-log plots of the relaxation timescale (τ, determined by the reciprocal of the frequency at the ε'' peak ω_p) *versus* the inverse temperature of PE-OPh and PE-Naph are given in the Fig. S7.† In both cases, the experimental results can be well fitted by the Vogel–Fulcher–Tammann (VFT) equation:[53,54] $\tau = \tau_0 \times \exp(B/(T - T_0))$, where τ_0 is the relaxation time in the limit of high temperature, B is a constant, and T_0 is the Vogel temp-

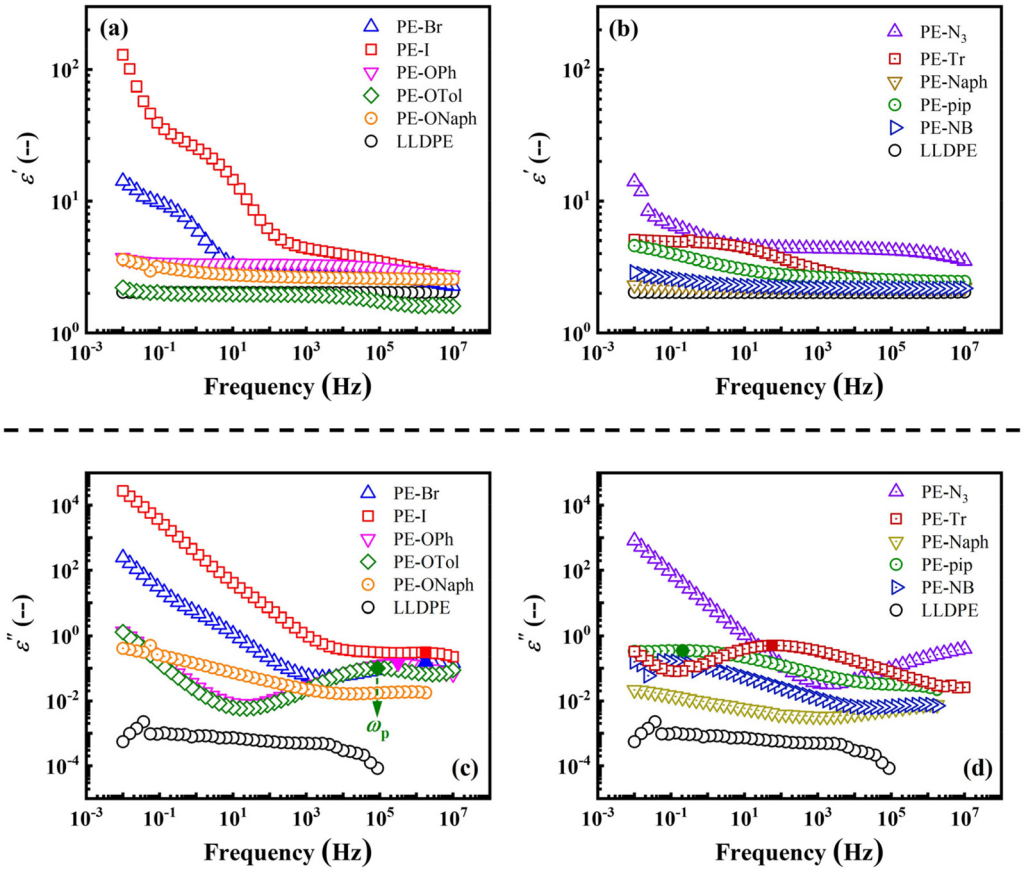

Fig. 2 Double logarithmic plots of (a) and (b) ε' and (c) and (d) ε'' *versus* frequency for the synthesized PE derivatives. LLDPE is employed as a basis for comparison. The position of the ε'' peak is indicated by a solid symbol and the frequency at the ε'' peak is denoted as ω_p.

erature. The fitting results suggest that the detected ε'' peaks are related to segment relaxation rather than whole chain relaxation.[55] The characteristic temperatures of PE-OPh and PE-Naph corresponding to τ of 100 s ($T_{\tau=100\ s}$) were extrapolated to be −10.7 °C and 39.1 °C, respectively. For PE-OPh, $T_{\tau=100\ s}$ is higher than its T_g of −24.4 °C obtained by DSC, while for PE-Naph, $T_{\tau=100\ s}$ is slightly lower than its T_g of 41.1 °C. This slowed segment mobility may lead to a slower polarization, possibly responsible for the decrease in the ε' of PE-OTol and PE-Tr in the high-frequency region. The segment dynamics is also related to the ω_p. When the substituents delay segment relaxation, the ω_p shifts toward low-frequency, requiring a longer timescale to polarize in large dimensions, *i.e.*, dipolar polarization, resulting in a high ε'. For example, the onset of the increase in ε' occurs with decreasing frequency due to the respective ω_p of PE-OPh, PE-Tr, and PE-pip (see Fig. 2(c), (d) and Table S1†).

We then compared the variable-temperature dielectric results of selected PE derivatives to understand the dependence of segment relaxation and polarization behaviors on temperature. Such understanding is crucial, especially when considering the operation conditions of dielectric devices, such as film capacitors and electronic packaging materials, which may involve high temperatures.

Fig. 3 shows the ε' ((a) and (c)) and ε'' ((b) and (d)) *versus* frequency plots obtained from 0 to 120 °C, revealing distinct trends. The ε' of PE-OPh shows a slight increase in the range of 10^5–10^7 Hz, rising from approximately 2.52 to 3.36 at 10^5 Hz as the temperature increases from 0 to 40 °C (before its T_m). However, the ε' of the melt of PE-OPh at 10^5 Hz remains almost constant at 4.0 under the subsequent heating from 80 to 120 °C. On the other hand, ε' at low frequency (10^{-2} to 10^1 Hz) increases with temperature, ranging from 3.16 at 0 °C to 24.7 at 120 °C for the measured ε' at 10^{-2} Hz. In contrast to PE-OPh, the ε' of PE-Naph increases with temperature over a wide frequency range above its T_g. In particular, at low frequency, the ε' at 10^{-2} Hz increased from 2.26 at 0 °C to 34.48 at 120 °C, surpassing that of PE-OPh. While polymers with benzene ring groups are generally considered to be less polarizable due to weak chain mobility and have lower ε' and ε'', it was found that the ε' and ε'' of PE-Naph with two aromatic rings were higher than those of PE-OPh at a given temperature. In other words, although the steric hindrance of PE-Naph is larger, the chain mobility is better, which can be attributed to its lower crystallinity.

Fig. 4(a) and (b) show the temperature dependence of the ε' at 10^3 and 10^7 Hz, respectively. PE derivatives of PE-Br, PE-I, PE-OPh, and PE-Naph all exhibit a similar temperature dependence of the ε' (refer to their plots of ε' *versus* frequency

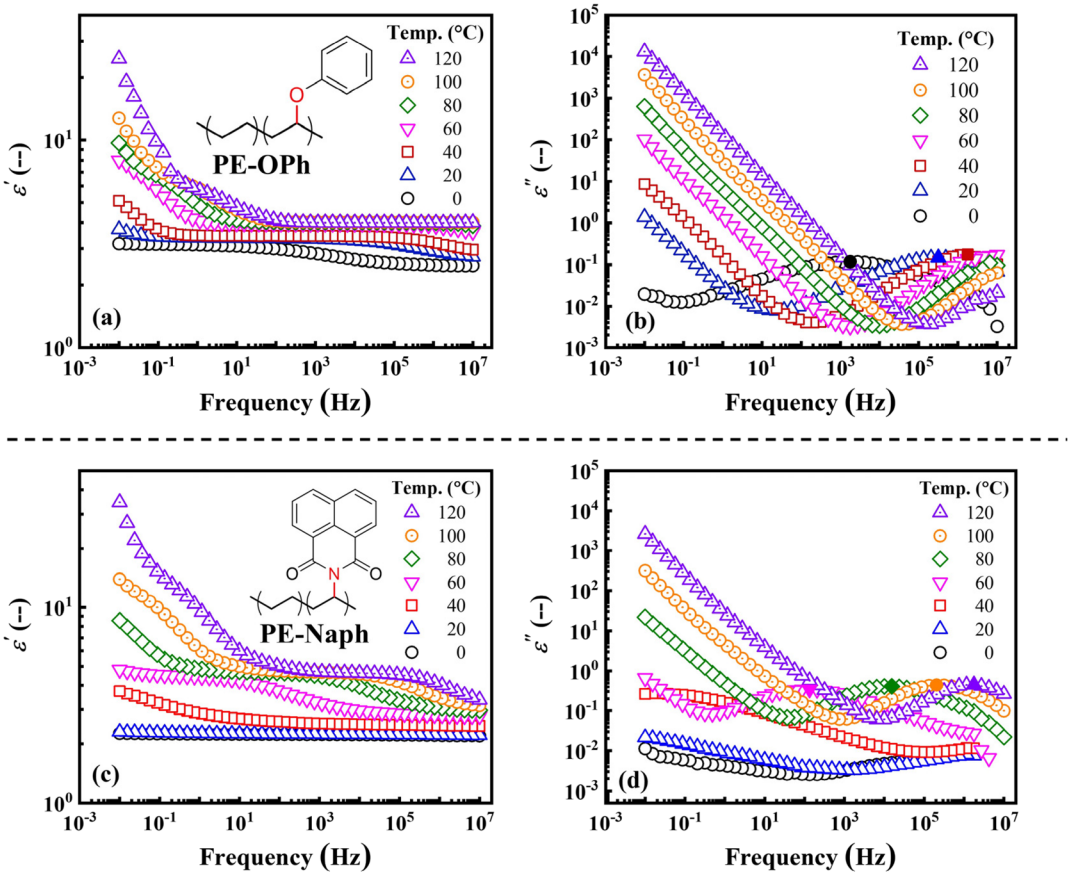

Fig. 3 Temperature dependence of the measured dielectric properties of the PE derivatives PE-OPh (top) and PE-Naph (bottom), including the log–log plots of ε' ((a) and (c)) and ε'' ((b) and (d)) *versus* frequency, respectively. The position of the ε'' peak is indicated by a solid symbol.

obtained at various temperatures in Fig. S8†), whereas the ε' of LLDPE is almost independent of the temperature. The results indicate a more pronounced increase in ε' with temperature for PE derivatives before reaching their respective T_m. Further investigations focusing on chain dynamics are required to reveal the mechanism by which functional groups influence the temperature dependence of ε'.

Dielectric properties of the blends of PE derivatives with LLDPE

One drawback of our PE derivatives is the elevated ε'', reaching about 10^{-1} (as observed in PE-Br, PE-I, and PE-OPh in Fig. 2(c)), which is two orders of magnitude higher than that of LLDPE (around 10^{-3}). ε'' is a crucial indicator for assessing

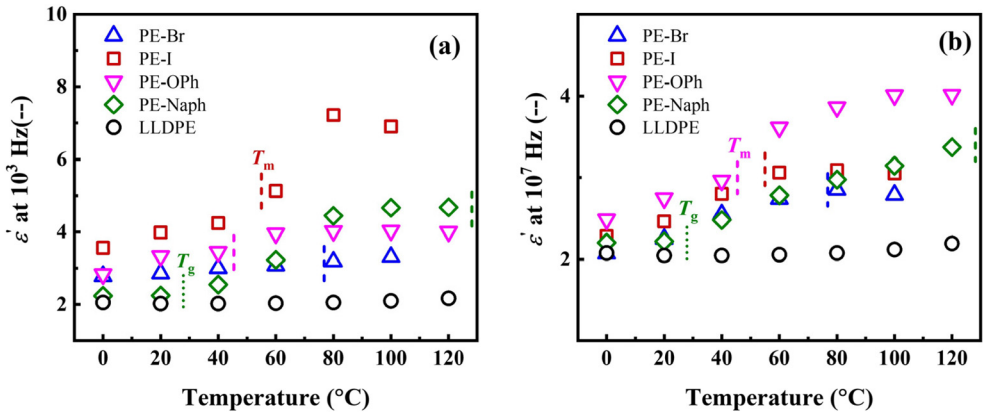

Fig. 4 Temperature dependence of the ε' measured at (a) 10^3 and (b) 10^7 Hz, respectively. The respective T_g and T_m were indicated in the plots.

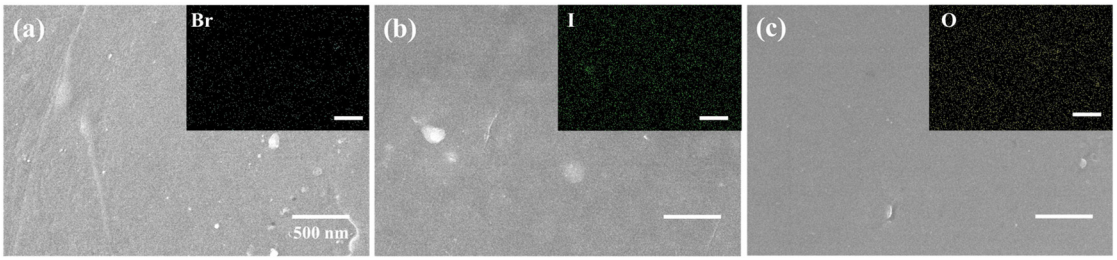

Fig. 5 SEM images of (a) PE-Br/LLDPE, (b) PE-I/LLDPE, and (c) PE-OPh/LLDPE blends. The EDX mapping results of (a) bromine, (b) iodine, and (c) oxygen are shown in the inset images. The scale bar corresponds to 500 nm. The content of PE derivatives is 5.9 wt% for all the three blends.

the performance of dielectric polymers. Generally, a ε'' below 10^{-2} is considered effective for applications, and some high-performance dielectric materials have reported values around 10^{-3}.[56,57] In this study, the synthesized PE derivatives, namely PE-Br, PE-I, and PE-OPh with higher ε', were blended with the low-ε'' LLDPE at 200 °C (in the molten state) to prepare polymer blends with both high ε' and low ε''. The relatively low degree of functionalization (18 mol%) was expected to ensure good interfacial compatibility between the three PE derivatives and the LLDPE matrix. To maintain low ε'' in these blends, a low concentration of 5.9 wt% was used for the PE derivatives. The SEM and EDX mapping images of the blends of PE-Br, PE-I, and PE-OPh with LLDPE are shown in Fig. 5(a)–(c) (the determined elemental composition is listed in Table S2†), demonstrating the uniform dispersion of PE derivatives in the matrix without phase separation at the micrometer scale.

The determined T_ds of the three blends were all above 400 °C (see Table 2, and the TGA curves are shown in Fig. S9†), indicating their good thermal stability. To reveal the effect of PE derivatives on the crystallization behavior of the LLDPE matrix, their DSC traces were compared, as shown in Fig. 6. Interestingly, the three PE derivatives were found to have the ability to induce crystallization of the LLDPE matrix at a higher T_c (see Fig. 6(a)), increasing from 107.4 °C in LLDPE to 108.4–108.6 °C in the blends (see Table 2). Although the T_m during subsequent heating (Fig. 6(b)) was nearly identical to that of LLDPE, the crystallinity of the LLDPE matrix increased after blending with PE-I and PE-OPh as their higher melting enthalpy normalized to the LLDPE content ($\Delta H_{m,n}$). The melting enthalpy of the reference material of LLDPE is detailed in Table 1. In contrast to the single melting peak of LLDPE, small shoulder peaks were detected in the heating curves of the blends (indicated by the arrows in Fig. 6(b)), suggesting the formation of some crystals with high T_m (or thicker lamellae). Furthermore, no crystallization or melting peak of the used PE derivatives was evident in the DSC traces. Thus, the selected PE derivatives induce the crystallization of LLDPE but do not crystallize by themselves. Given that the crystal diffractions of the blends are consistent with that of LLDPE (see 1-D WAXD curves in Fig. S10†), we conclude that the PE derivatives

Table 2 Determination of the thermal properties of the PE-Br/LLDPE, PE-I/LLDPE, and PE-OPh/LLDPE blends. The content of PE derivatives is 5.9 wt% for all the three blends

Sample	T_c (°C)	ΔH_c (J g^{-1})	T_m (°C)	ΔH_m (J g^{-1})	$\Delta H_{m,n}$ [a] (J g^{-1})	T_d (°C)
PE-Br/LLDPE	108.6	57.9	120.4	57.2	60.8	426.4
PE-I/LLDPE	108.6	89.6	120.5	91.9	97.7	433.0
PE-OPh/LLDPE	108.5	101.5	120.5	101.3	107.7	410.0

[a] The melting enthalpy normalized to the LLDPE content.

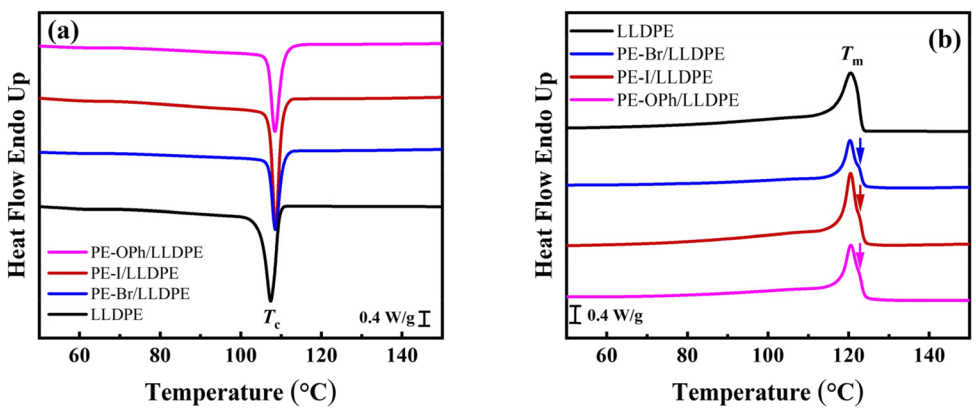

Fig. 6 (a) Cooling and (b) second heating DSC traces of the PE-Br/LLDPE, PE-I/LLDPE, and PE-Naph/LLDPE blends, with LLDPE employed as the reference. The shoulder peaks in the heating traces are indicated by arrows. The PE derivative content is 5.9 wt% for all the three blends.

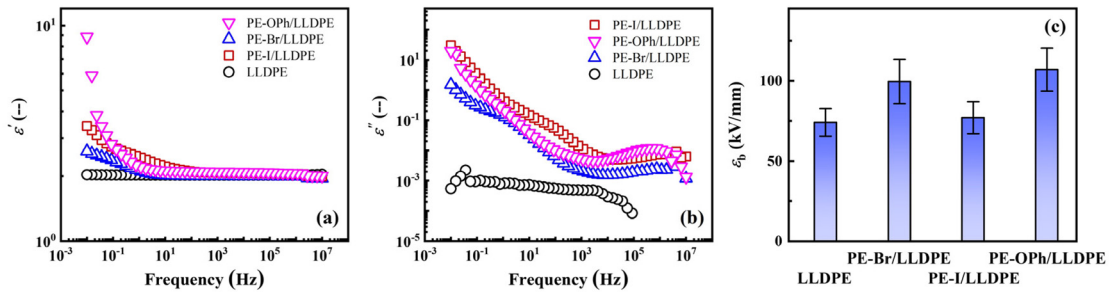

Fig. 7 Double logarithmic plots of (a) ε' and (b) ε'' *versus* frequency obtained from the PE-Br/LLDPE, PE-I/LLDPE, and PE-OPh/LLDPE blends, with a LLDPE matrix used as a reference. (c) Comparison of ε_b of these blends with the LLDPE matrix. The PE content is 5.9 wt% for all the three blends.

are located in the amorphous region and are not involved in the crystal lattice of LLDPE.

The dielectric properties of the three blends at room temperature are presented in Fig. 7, demonstrating the benefits of blending with LLDPE. Blending significantly reduced ε'' by more than one order of magnitude compared to the PE derivatives themselves (Fig. 2(c)). The magnitude of the ε'' peak was lowered to approximately 10^{-2} (Fig. 7(b)), meeting commercial quality standards. By comparing the dielectric properties of the blend of reactant EVA (the vinyl acetate content of 18 mol%) with LLDPE (refer to Fig. S11†), it was found that ε' was effectively enhanced for PE-Br/LLDPE, PE-I/LLDPE, PE-OPh/LLDPE at low frequencies by inserting the substituents *via* the Mitsunobu functionalization method. Notably, even at low concentrations (5.9 wt%), the PE derivatives enhance ε' at frequencies below 10 Hz, reaching up to 8.9 for PE-OPh/LLDPE at 0.01 Hz (Fig. 7(a)). Specifically, the ε' of PE-OPh exhibited weak frequency dependence, remaining constant at *ca.* 3.40, but a noticeable decrease in ε' was observed in the 10^{-2}–10^{0} range for the PE-OPh/LLDPE blend. On the other hand, the ε'' of PE-Br and PE-I decreased by approximately one order of magnitude after blending with LLDPE, but the ε'' of PE-OPh/LLDPE was about three orders of magnitude lower than that of PE-OPh (Fig. 7(b)). Moreover, the ε'' peak position of studied samples remained unchanged after blending with LLDPE, indicating that the LLDPE blending does not affect the relaxation time (the reciprocal of the ε'' peak position) but only reduces ε''.

More importantly, we noticed that by adding small amounts of PE derivatives, the ε_b of the LLDPE matrix also effectively improved (see Fig. 7c and Table 3), with the ε_b of PE-OPh/LLDPE approximately 1.4 times that of the LLDPE matrix. ε_b is a critical factor in device performance, and an increase in the working electric field often results in better dielectric properties until the material undergoes breakdown. Based on the literature,[18,58] the chain mobility plays a crucial role in determining the ε_b. Recently, the ε_b of PEI/PI blends was reported to be higher than that of respective homopolymers, attributed to the higher molecular chain packing density in the blend.[59] Hence, enhancing ε_b in polymeric materials involves forming a more dense chain packing. The high ε_b observed in PE-Br/LLPDE and PE-OPh/LLDPE can be ascribed

Table 3 Determination of the dielectric properties of the PE-Br/LLDPE, PE-I/LLDPE, and PE-OPh/LLDPE blends. The content of PE derivatives is 5.9 wt% for all the three blends

Sample	ε'@10^{-2} Hz	ε'@10^{0} Hz	ε'@10^{3} Hz	ω_p [a] (Hz)	ε''_p [b]	ε_b [c] (kV mm^{-1})
PE-Br/LLDPE	2.38	2.11	2.01	4.2×10^{6}	3.0×10^{-3}	99.5 ± 13.9
PE-I/LLDPE	2.75	2.44	2.08	4.2×10^{6}	9.2×10^{-3}	76.9 ± 9.9
PE-OPh/LLDPE	2.81	2.21	2.10	7.5×10^{5}	1.2×10^{-2}	106.9 ± 13.4

[a] Corresponding frequency at the ε'' peak. [b] Peak value in the plot of ε'' *versus* frequency. [c] The average breakdown strength of the studied blends at room temperature.

to the higher crystallinity of the LLDPE component induced by the PE derivatives. This is supported by the fact that PE-OPh/LLDPE with the highest $\Delta H_{m,n}$, as shown in Table 2, exhibits the highest ε_b. However, PE-I/LLDPE exhibits a lower ε_b than PE-Br/LLDPE despite its higher $\Delta H_{m,n}$, which is possibly caused by the large radius of iodine, and the amorphous region containing molecular chains of PE derivatives and LLDPE may form a denser packing. As no significant T_m or crystal reflection corresponding to PE-Br, PE-I, and PE-OPh themselves (those of the LLDPE matrix) were observed in the DSC (Fig. 6) and 1-D WAXD (Fig. S10†) curves, respectively, the crystallization of PE derivatives in the blends is negligible. Based on the WAXD result, the unit cell of PE-I is very different from that of LLDPE, yet the PE-I/LLDPE blend exhibits a typical orthorhombic unit cell of PE. Therefore, the molecular chains of PE-Br, PE-I, and PE-OPh are located in the amorphous region for the three blends. A higher ε_b should be obtained if a certain dense structure is established in the amorphous region through the interactions between the PE derivatives and LLDPE chains.

These experimental results clearly demonstrated that the selected PE derivatives can successfully improve the ε_b of polymer blends. This approach is expected to be advantageous for polymer/nano-filler composite systems, as the functional groups on the PE derivatives allow tunable interfacial compatibility or interactions between polymer chains and nano-fillers.

The temperature dependence of the ε and ε'' of the PE-OPh/LLDPE blend, which exhibits the highest ε' among the three blends, was investigated to assess its suitability for high-temperature applications. As depicted in Fig. 8(a), ε' demonstrates a significant increase at elevated temperatures, particularly in the low-frequency region. This differs from LLDPE, where ε' remains constant until the melting temperature (refer to Fig. S8(e)†). The increase in ε' diminishes from the low-frequency to high-frequency regions during the heating process, suggesting that the chain mobility of the added PE-OPh is not constrained by the LLDPE matrix, leading to observable polarization behavior. This behavior is consistent with that observed for PE-Br/LLDPE and PE-I/LLDPE (see Fig. S12†). In Fig. 8(b), two ε'' peaks were detected in the measured frequency range (similar peaks were observed for PE-Br/LLDPE and PE-I/LLDPE; see Fig. S12†). The first peak, ε''_1, occurs between 0.06 Hz and 315.90 Hz, while the second peak, ε''_2, is located between 4.2×10^3 Hz and 7.5×10^5 Hz. The relaxation time of ε''_1 is longer than that of ε''_2 due to the lower ω_p. Upon heating, both ε''_1 and ε''_2 peaks gradually shift toward higher frequencies, indicating a decrease in their respective τ with increasing temperature. Fig. 8(c) further illustrates a more pronounced temperature dependence of ε' at both 1 Hz and 1 kHz for all three PE derivatives compared to LLDPE as temperature increases. The similar temperature dependence of τ determined by the ε''_1 peak of the three blends is shown in Fig. 8(d). The VFT equation provides a good fit for the three plots shown in Fig. 8(d), confirming that the detected ε''_1 peaks are related to segmented relaxation. The characteristic $T_{\tau=100\ s}$ were determined to be −3.4 °C, −12.4 °C, and 14.1 °C for PE-Br/LLDPE, PE-I/LLDPE, and PE-OPh/LLDPE, respectively. Unfortunately, it is difficult to compare the respective $T_{\tau=100\ s}$ with T_g for the three blends, as their T_gs could not be determined from the DSC traces. Given that several electric components operate at elevated temperatures due to the waste heat generated during service, blending with PE derivatives presents potential for dielectric applications of polyolefin-based materials.

Influence of PE derivatives on the mechanical properties of LLDPE-based blends

Depending on the application, the mechanical properties required for polymeric materials may vary. For instance, electrical devices demand sufficient strength and flexibility for effective protection. Polymer blending serves as a valuable

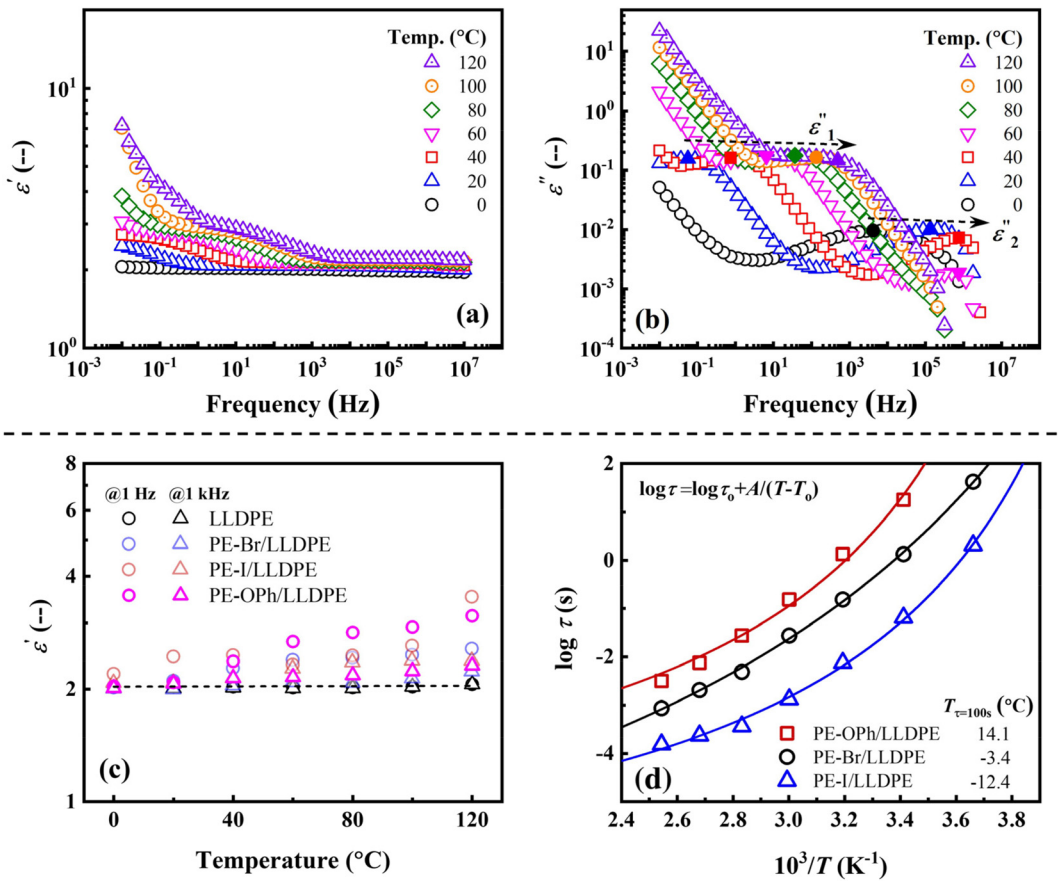

Fig. 8 Log–log plots of (a) ε' and (b) ε'' *versus* frequency obtained at different temperatures for the PE-OPh/LLDPE blend. The ε''_1 and ε''_2 peaks are indicated by the solid symbols. (c) Temperature dependence of ε' of PE-Br/LLDPE, PE-I/LLDPE, and PE-OPh/LLDPE. LLDPE is used as the reference material. (d) The semi-log plots of τ, determined by the ε''_1 peak, *versus* temperature for the three studied blends. The solid lines are the fitting results by the VFT equation, which is inserted in the figure. The determined $T_{\tau=100\ s}$ is listed in the figure. The content of PE derivatives is 5.9 wt% for all the three blends.

method for fine-tuning these mechanical properties. In this section, we aim to describe the influence of PE derivatives on the mechanical properties and the underlying mechanism when blended with an LLDPE matrix. The results obtained will contribute to the development of polymeric materials with superior dielectric and flexibility characteristics.

Fig. 9 shows the comparison results of the three PE derivatives PE-Br, PE-I, and PE-OPh and their blends. Due to the low crystallinity of PE-Br, PE-I, and PE-OPh, their engineering stress–strain plots reveal significant flexibility in contrast to LLDPE (refer to Fig. S13†). Specifically, the strain-at-break is higher, but the modulus and strength are noticeably weaker (Table S3†). Surprisingly, Young's modulus for the studied blends reached 54–59 MPa, approximately 1.5 times that of the LLDPE matrix. Moreover, the strain-at-break of both PE-Br/LLDPE and PE-OPh/LLDPE exceeded 1000% (similar to elastomers' results[60]), which is twice that of the LLDPE matrix. These results highlight that PE derivatives can enhance not only the modulus (and stress-at-break) but also flexibility. Among the three PE derivatives, PE-Br exhibits the greatest enhancement of the mechanical properties of the LLDPE matrix, while PE-I only improved Young's modulus with a negligible effect on the strain-at-break/stress-at-break. The excellent mechanical properties of PE-Br/LLDPE and PE-OPh/LLDPE are demonstrated by the strain-at-break and stress-at-break, which are comparable to those of the blend of LLDPE with the reactant EVA (a commonly used elastomer) at a same composition of 5.9 wt% (see Table S3†).

When two polymers are incompatible, their blends are prone to fracture easily under the applied deformation owing to their phase separation behavior. Based on the EDX mapping results (Fig. 5), no evident phase domain is observed at the microscale for the three studied blends. In the polymer blends[61] or copolymer systems,[62–64] DMA is a common method to study the presence of (micro-)phase separation. The temperature dependence of the dynamic storage (E') and loss (E'') moduli was compared to clarify whether the microphase domain exists (as shown in Fig. 10). Only a single $T_{g,DMA}$ was detected in the LLDPE matrix, while two $T_{g,DMA}$s were found in all three blends, implying significant differences between the microstructures of the LLDPE matrix and the studied blends. Moreover, PE derivatives (PE-Br, PE-I, and PE-OPh) all exhibit only one $T_{g,DMA}$ in their DMA results, suggesting weak or no microphase separation structure, which is supported by the extremely weak signal observed in the 1-D SAXS plots (Fig. S14†) obtained by quenching from 200 °C using a liquid nitrogen bath for the three PE derivatives. The weak SAXS signals also suggest that long-rang ordered morphologies may not have formed. The E'' peak in the DMA plots of the three blends within 30–50 °C indicates that a certain structure is established, possibly due to crystallinity or microphase separation. Barbosa *et al.* found that low-temperature shifts of the E'' peaks and the disappearance of one peak occurred in modified EVA quenched using a liquid nitrogen bath, usually exhibiting less crystallinity.[65] However, the effect of crystallinity on the E''-T plot is controversial. Some literature reported only shifts in peak position without peak formation or disappearance when crystallinity changed due to blending[66,67] or copolymerization.[68,69] Unfortunately, preparing amorphous blends of LLDPE with PE derivatives to clarify the microphase separation *via* SAXS is challenging due to easy crystallization and a low T_g of the LLDPE matrix (reported as *ca.* −30 °C (ref. 70) and −130 °C (ref. 71 and 72) by different groups using linear diatometry), as evidenced by the DSC cooling traces of the studied blends at approximately 50 °C min^{-1} (see Fig. S15†). Crystallization of PE was still observed even at a cooling rate of 1×10^6 K s^{-1} using Flash DSC.[73] Thus, the obtained 1-D SAXS profile may contain signals from both crystal and possible microphase separation, making it difficult to elucidate the presence of a microphase separation structure. We currently believe that a certain microstructure forms in the LLDPE blend with PE derivatives, leading to a new E'' peak formed at 30–50 °C, but we cannot determine its nature. Considering that the synthesized PE derivatives are random

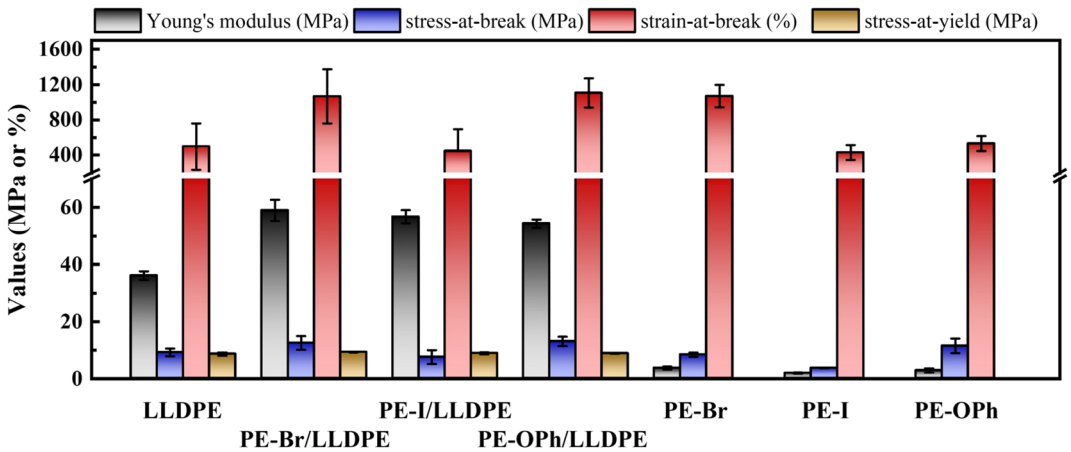

Fig. 9 Comparison results of the mechanical properties of the PE derivatives PE-Br, PE-I, and PE-OPh and their blends. The content of PE derivatives is 5.9 wt% for the blends. LLDPE is used as a reference.

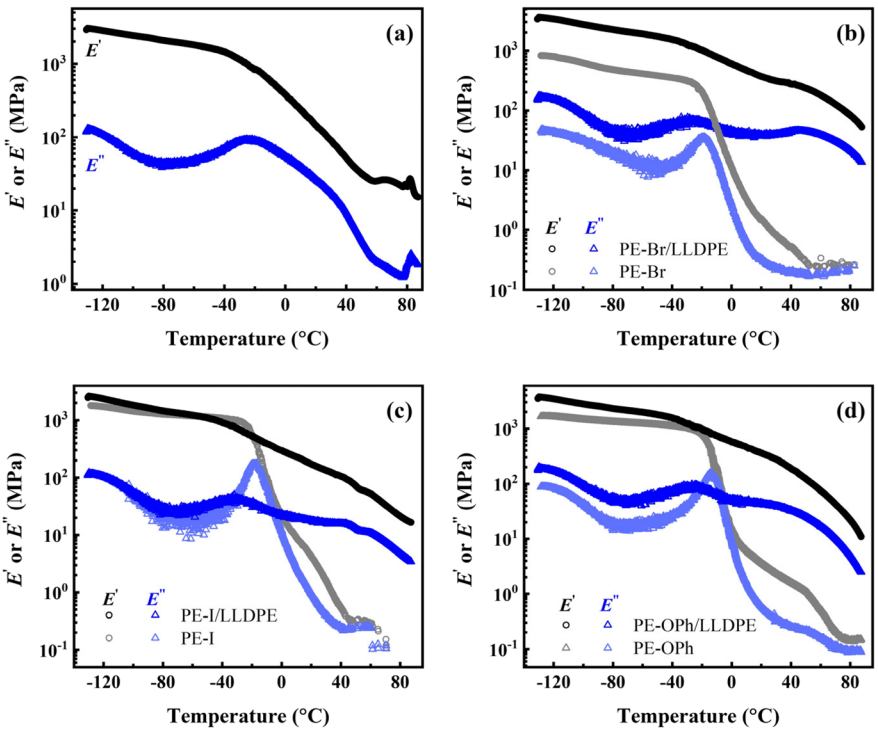

Fig. 10 DMA curves of the studied PE derivatives and their blends: (a) LLDPE matrix, (b) PE-Br and PE-Br/LLDPE, (c) PE-I and PE-I/LLDPE, and (d) PE-OPh and PE-OPh/LLDPE. The content PE derivatives is 5.9 wt% for the blends.

copolymers, we suspect this microstructure is related to microphase separation when the difference in chemical compatibility between the PE monomer and the substituents is sufficiently large.

As shown in Fig. 10(b)–(d), the $T_{g,DMA}$ in the range of −32 to −24 °C closely matches that of the respective PE derivatives for all the studied blends (see Table S4†), while the other $T_{g,DMA}$ of 30–50 °C is higher than that of the PE derivatives and the LLDPE matrix. The former one may be explained by the $T_{g,DMA}$ reducing to a value closer to that of the PE backbone (reported as −30 °C (ref. 70)) due to the high fraction of the LLDPE matrix. The higher $T_{g,DMA}$ may be attributed to the specific microstructure formed after blending with LLDPE, contributing to the higher E' at elevated temperatures. This microstructure may act as a physical crosslinking network during the uniaxial deformation at room temperature, endowing the blends with a higher Young's modulus than that of the LLDPE matrix at near crystallinity. On the other hand, the amorphous molecules of the PE derivative provide flexibility to the blends, allowing them to withstand greater strain.

The formed microstructure can also explain the excellent dielectric properties of the blends. The amorphous chain segments of PE derivatives with better mobility are more likely to undergo polarization, contributing to high ε' at elevated temperatures. Moreover, the specific microstructure can result in a denser packing of the amorphous chains of PE derivatives and LLDPE, thereby enhancing the ε_b. Unfortunately, the microstructures could not be further investigated using the SAXS technique because the scattering signal is difficult to distinguish from the signal of the LLDPE crystals. More studies are needed to explore the evolution of the microstructure in detail under the applied stretching/electric fields for PE derivative-based systems, providing new insights into the modulation of the dielectric properties of polymeric materials.

Conclusions

In this work, ten PE derivatives obtained by the post-functionalization reaction from the same commercial EVA precursors (18 mol% functional group contents) were employed to compare the impact of functional group structures on the microstructures, thermal properties, and mechanical properties. This approach allows the examination of differences in chemical structures and their effects on the dielectric properties, as exemplified by PE derivatives PE-OPh and PE-OTol. Meanwhile, it facilitates the exploration of dielectric properties in novel polymers containing complex functional groups. Experimental results show a significant influence of the structure of functional groups on the ε' of the PE derivatives. PE-Br and PE-I exhibit ε's one and two orders of magnitude higher than that of LLDPE at low frequencies, respectively. PE-N_3 containing azide functional groups displays a ε' greater than 3.0 over the measured frequency range, while PE-Naph containing a naphthalimide structure exhibits a low ε' almost identical to that of LLDPE. The comparison of the crystal structure and

thermal properties reveals that PE-I and PE-Naph have a unit cell structure different from that of LLDPE, and the T_m of PE-Naph is the highest among all the samples. Our strategy demonstrates potential for developing novel dielectric polymers with high melting temperatures and ε' through an in-depth study of the relationship between the microstructure and properties.

PE-Br/LLDPE, PE-I/LLDPE, and PE-OPh/LLDPE blends with a 5.9 wt% fraction of PE derivatives were successfully prepared, and the PE backbone in the molecular chains ensured good compatibility between the PE derivatives and the LLDPE matrix. The ε'' of the PE derivatives was reduced by 1–2 orders of magnitude through blending with LLDPE, while the added PE derivatives enhanced the ε' compared to LLDPE at frequencies below 10 Hz. Notably, the blends exhibit a more pronounced temperature dependence of ε' compared to LLDPE, with ε' increasing as the temperature rises. Moreover, PE-Br and PE-OPh have been shown to increase the ε_b of blends, and the ε_b of PE-OPh/LLDPE is 1.4 times higher than that of the LLDPE matrix. The PE derivatives PE-Br, PE-I, and PE-OPh induce the crystallization of the LLDPE matrix, as evidenced by both T_c and $\Delta H_{m,n}$, although they are not involved in the unit cell. The PE derivatives enhance the mechanical properties of the blends, including Young's modulus, stress-at-break, and strain-at-break. Surprisingly, PE-Br/LLDPE and PE-OPh/LLDPE exhibit elastomer-like behavior, reaching a strain-at-break of more than 1000%. These results demonstrate that adding a small amount of PE derivatives can simultaneously enhance the dielectric properties, mechanical properties, and crystallization temperature of the commercial LLDPE matrix, offering considerable potential for large-scale production and economic value.

Data availability

The data supporting this article have been included as part of the ESI.†

Conflicts of interest

The authors declare no competing financial interests.

Acknowledgements

This work was financially supported by the Beijing Municipal Natural Science Foundation (Grant No. 2232074) and the National Natural Science Foundation of China (Grant No. 22175188). The authors also acknowledge the assistance of Prof. Ming Tian (Beijing University of Chemical Technology) and Prof. Nanying Ning (Beijing University of Chemical Technology) in dielectric breakdown strength measurements.

References

1 F. Kremer and A. Schönhals, *Broadband Dielectric Spectroscopy*, Springer-Verlag Berlin Heidelberg, New York, 2003.
2 L. Zhu, *J. Phys. Chem. Lett.*, 2014, **5**, 3677–3687.
3 S. Wang, C. Yang, X. Li, H. Jia, S. Liu, X. Liu, T. Minari and Q. Sun, *J. Mater. Chem. C*, 2022, **10**, 6196–6221.
4 R. Cheng, Y. Wang, R. Men, Z. Lei, J. Song, Y. Li and M. Guo, *iScience*, 2022, **25**, 104837.
5 R. G. Lorenzini, W. M. Kline, C. C. Wang, R. Ramprasad and G. A. Sotzing, *Polymer*, 2013, **54**, 3529–3533.
6 T. D. Huan, S. Boggs, G. Teyssedre, C. Laurent, M. Cakmak, S. Kumar and R. Ramprasad, *Prog. Mater. Sci.*, 2016, **83**, 236–269.
7 D. W. van Krevelen and K. Te Nijenhuis, *Properties of Polymers*, Elsevier, The Netherlands, 2009.
8 P. Barber, S. Balasubramanian, Y. Anguchamy, S. Gong, A. Wibowo, H. Gao, H. Ploehn and H.-C. Zur Loye, *Materials*, 2009, **2**, 1697–1733.
9 Prateek, V. K. Thakur and R. K. Gupta, *Chem. Rev.*, 2016, **116**, 4260–4317.
10 M. Zhang, B. Li, J. J. Wang, H. B. Huang, L. Zhang and L. Q. Chen, *Adv. Mater.*, 2021, **33**, e2008198.
11 L. Zhu and Q. Wang, *Macromolecules*, 2012, **45**, 2937–2954.
12 X.-J. Liu, M.-S. Zheng, G. Chen, Z.-M. Dang and J.-W. Zha, *Energy Environ. Sci.*, 2022, **15**, 56–81.
13 Z. Zhu, G. Rui, R. Li, H. He and L. Zhu, *Macromolecules*, 2021, **54**, 9879–9887.
14 J.-Y. Ren, Q.-F. Ouyang, G.-Q. Ma, Y. Li, J. Lei, H.-D. Huang, L.-C. Jia, H. Lin, G.-J. Zhong and Z.-M. Li, *Macromolecules*, 2022, **55**, 2014–2027.
15 E. Baer and L. Zhu, *Macromolecules*, 2017, **50**, 2239–2256.
16 W. Fan, Y. Du, Z. Yuan, P. Zhang and W. Fu, *Macromolecules*, 2023, **56**, 6482–6491.
17 Y. Chen, X. Chen, Y. Wang, Z. Nie, X. Wang, J. Tan, Y. Zhuang, X. Liu and X. Wang, *Macromolecules*, 2023, **56**, 9379–9388.
18 C.-Y. Liu, D.-L. Li, Y. Li, L. Xu, X. Meng, G.-J. Zhong, H.-D. Huang and Z.-M. Li, *Macromolecules*, 2022, **55**, 9680–9689.
19 A. Yanaka, W. Sakai, K. Kinashi and N. Tsutsumi, *RSC Adv.*, 2020, **10**, 15740–15750.
20 S. Zhang, H. Hu, H. Yu, Y. Huang and J. Yang, *Macromol. Res.*, 2017, **25**, 381–385.
21 G. Chen, Y. Liang, D. Xiang, S. Wen and L. Liu, *J. Mater. Sci.*, 2017, **52**, 10321–10330.
22 D. Ai, H. Li, Y. Zhou, L. Ren, Z. Han, B. Yao, W. Zhou, L. Zhao, J. Xu and Q. Wang, *Adv. Energy Mater.*, 2020, **10**, 1903881.
23 J. Wei, Z. Zhang, J. K. Tseng, I. Treufeld, X. Liu, M. H. Litt and L. Zhu, *ACS Appl. Mater. Interfaces*, 2015, **7**, 5248–5257.
24 H. Luo, F. Wang, R. Guo, D. Zhang, G. He, S. Chen and Q. Wang, *Adv. Sci.*, 2022, **9**, e2202438.
25 Z. Chu, L. Liu, Y. Lou, R. Zhao, Z. Ma and Y. Li, *Ind. Eng. Chem. Res.*, 2020, **59**, 4459–4471.

26 Z. Chu, L. Liu, Y. Liao, W. Li, R. Zhao, Z. Ma and Y. Li, *Polymer*, 2020, **203**, 122773.
27 Q. K. Feng, S. L. Zhong, J. Y. Pei, Y. Zhao, D. L. Zhang, D. F. Liu, Y. X. Zhang and Z. M. Dang, *Chem. Rev.*, 2022, **122**, 3820–3878.
28 S. Cheng, Y.-S. Li, J.-J. Liang and Q. Li, *Acta Polym. Sin.*, 2020, **51**, 469–483.
29 B. Fan, M. Zhou, C. Zhang, D. He and J. Bai, *Prog. Polym. Sci.*, 2019, **97**, 101143.
30 K. Omote, H. Ohigashi and K. Koga, *J. Appl. Phys.*, 1997, **81**, 2760–2769.
31 X. Chen, H. Qin, X. Qian, W. Zhu, B. Li, B. Zhang, W. Lu, R. Li, S. Zhang, L. Zhu, F. Domingues Dos Santos, J. Bernholc and Q. M. Zhang, *Science*, 2022, **375**, 1418–1422.
32 Z. Cui, N. T. Hassankiadeh, Y. Zhuang, E. Drioli and Y. M. Lee, *Prog. Polym. Sci.*, 2015, **51**, 94–126.
33 M. Li, H. J. Wondergem, M. J. Spijkman, K. Asadi, I. Katsouras, P. W. Blom and D. M. de Leeuw, *Nat. Mater.*, 2013, **12**, 433–438.
34 A. J. Lovinger, *Macromolecules*, 2002, **15**, 40–44.
35 R. Hasegawa, Y. Takahashi, Y. Chatani and H. Tadokoro, *Polym. J.*, 1972, **3**, 600–610.
36 Z. Chu, R. Zhao, B. Wang, L. Liu, Z. Ma and Y. Li, *Macromolecules*, 2021, **54**, 3800–3809.
37 J.-T. Wang, Z. Chen, Y.-Q. Wang, Y.-F. Chu, M. Pan and L.-J. Dong, *Acta Polym. Sin.*, 2020, **51**, 1367–1373.
38 J. A. S. Puente, B. Rijal, L. Delbreilh, K. Fatyeyeva, A. Saiter and E. Dargent, *Polymer*, 2015, **76**, 213–219.
39 I. Šics, T. A. Ezquerra, F. J. BaltÁ Calleja, V. Tupureina and M. Kalninš, *J. Macromol. Sci., Part B: Phys.*, 2007, **39**, 761–774.
40 S. Srinivasan, *Fuel Cells: From Fundamentals to Applications*, Springer, New York, 2006.
41 J. O. M. Bookris, A. K. N. Reddy and M. Gamboa-Aldeco, *Modern Electrochemistry: Fundamentals of Electrodics*, Kluwer Academic, New York, 2nd edn, 2002.
42 C. Tan and C. Chen, *Angew. Chem., Int. Ed.*, 2019, **58**, 7192–7200.
43 Y. Zhang, T. Wang, J. Bai and W. You, *ACS Macro Lett.*, 2021, **11**, 33–38.
44 Y. Zhang, Y. Wang and W. You, *Acta Polym. Sin.*, 2023, **54**, 1836–1843.
45 Y. Zhang, Y. Wang and W. You, *J. Appl. Polym. Sci.*, 2023, **140**, e54711.
46 J. Mao, S. Wang, Y. Cheng, B. Xiao, L. Zhang, D. Ai, Y. Chen, W. Sun and J. Luo, *Chem. Eng. J.*, 2022, **444**, 136331.
47 C. Wu, A. A. Deshmukh, O. Yassin, J. Zhou, A. Alamri, J. Vellek, S. Shukla, M. Sotzing, R. Casalini, G. A. Sotzing and Y. Cao, *Proc. Natl. Acad. Sci. U. S. A.*, 2021, **118**, e2115367118.
48 A. A. Deshmukh, C. Wu, O. Yassin, A. Mishra, L. Chen, A. Alamri, Z. Li, J. Zhou, Z. Mutlu, M. Sotzing, P. Rajak, S. Shukla, J. Vellek, M. A. Baferani, M. Cakmak, P. Vashishta, R. Ramprasad, Y. Cao and G. Sotzing, *Energy Environ. Sci.*, 2022, **15**, 1307–1314.
49 P. Kaner, C. Ruiz-Orta, E. Boz, K. B. Wagener, M. Tasaki, K. Tashiro and R. G. Alamo, *Macromolecules*, 2013, **47**, 236–245.
50 N. Naga, R. Arai, G. Kikuchi, A. Toyota, K. Noguchi, M. Sone, F. Shirae, T. Gotoh and H. Kurosu, *Polymer*, 2011, **52**, 4857–4866.
51 H. Janani, S. F. Marxsen, M. Eck, S. Mecking, K. Tashiro and R. G. Alamo, *ACS Macro Lett.*, 2024, 201–206, DOI: **10.1021/acsmacrolett.3c00639**.
52 J. Lu, Y. Zhang, J. Li, M. Fu, G. Zou, S. Ando and Y. Zhuang, *Macromolecules*, 2023, **56**, 2164–2174.
53 G. S. Fulcher, *J. Am. Ceram. Soc.*, 1925, **8**, 339–355.
54 G. Tammann and W. Hesse, *Z. Anorg. Allg. Chem.*, 2004, **156**, 245–257.
55 A. R. Brás, M. T. Viciosa, Y. Wang, M. Dionísio and J. F. Mano, *Macromolecules*, 2006, **39**, 6513–6520.
56 X. Zhang, D. Zhu, H. You, Y. Hashimoto, T. Miyata, P. Chammingkwan and T. Taniike, *ACS Appl. Electron. Mater.*, 2022, **4**, 1257–1265.
57 C. Zhang, X. He and Q. Lu, *Eur. Polym. J.*, 2023, **200**, 112544.
58 C.-Y. Liu, D.-L. Li, Z.-H. Wang, Y. Li, S.-Y. Zhou, L. Xu, G.-J. Zhong, H.-D. Huang and Z.-M. Li, *Macromolecules*, 2023, **56**, 1481–1491.
59 V. Jurečič, N. Novak, L. Fulanović and V. Bobnar, *Macromolecules*, 2023, **56**, 1097–1104.
60 Y.-L. Qin, P. Zhu, C.-X. Ouyang and X. Dong, *Chin. J. Polym. Sci.*, 2023, **42**, 87–96.
61 Y. Li, C. Zhang and S. Zheng, *Eur. Polym. J.*, 2011, **47**, 1550–1562.
62 M. Wang, L. Zhang and D. Ma, *Eur. Polym. J.*, 1999, **35**, 1335–1343.
63 J. T. Garrett, R. Xu, J. Cho and J. Runt, *Polymer*, 2003, **44**, 2711–2719.
64 T. A. Speckhard, G. V. Strate, P. E. Gibson and S. L. Cooper, *Polym. Eng. Sci.*, 2004, **23**, 337–349.
65 R. V. Barbosa, R. B. Neto, R. S. Mauler, C. J. P. Gorga, C. G. Schneider and A. G. Simanke, *J. Appl. Polym. Sci.*, 2005, **97**, 1371–1376.
66 A. R. Aragão Melo, E. Oliveira da Silva, L. R. Menezes and M. I. B. Tavares, *Polym. Test.*, 2018, **68**, 333–339.
67 P. A. Lovell, J. L. Stanford, Y. F. Wang and R. J. Young, *Macromolecules*, 1998, **31**, 834–841.
68 Z. Xu and S. Zheng, *Macromolecules*, 2007, **40**, 2548–2558.
69 Y. Miura, T. Kaneko, K. Satoh, M. Kamigaito, H. Jinnai and Y. Okamoto, *Chem. – Asian J.*, 2007, **2**, 662–672.
70 J. H. Magill, S. S. Pollack and D. P. Wyman, *J. Polym. Sci., Part A: Gen. Pap.*, 1965, **3**, 3781–3786.
71 P. R. Swan, *J. Polym. Sci.*, 1960, **42**, 525–534.
72 M. L. Dannis, *J. Appl. Polym. Sci.*, 1959, **1**, 121–126.
73 E. Zhuravlev, V. Madhavi, A. Lustiger, R. Androsch and C. Schick, *ACS Macro Lett.*, 2016, **5**, 365–370.